Journal of Inorganic Biochemistry 271 (2025) 112978

Contents lists available at ScienceDirect

Journal of Inorganic Biochemistry

journal homepage: www.elsevier.com/locate/jinorgbio

Exploring the anticancer properties of indenyl and allyl palladates through their interaction with nucleic acids☆

Tommaso Giani [a], Giannantonio Tomasi [a], Pablo A. Nogara [b], Laura Orian [c], Fabiano Visentin [d], Thomas Scattolin [c], Tarita Biver [a,*]

[a] Department of Chemistry and Industrial Chemistry, University of Pisa, Via G. Moruzzi 13, 56124 Pisa, Italy
[b] Federal Institute of Education, Science and Technology Sul-rio-grandense (IFSul), Av. Leonel de Moura Brizola, 2501, 96418-400 Bagé, RS, Brazil
[c] Department of Chemical Sciences, University of Padua, via Marzolo 1, 35131 Padova, Italy
[d] Department of Molecular Sciences and Nanosystems, Ca' Foscari University of Venice, Via Torino 155, 30174 Venezia-Mestre, Italy

ARTICLE INFO

Keywords:
Palladium complexes
Metallodrugs
Nucleic acids
Mechanism of action
G-quadruplexes
I-motif

ABSTRACT

In this work, we analyse the mechanistic features of the interaction of indenyl (**1-Ind**) and allyl (**2-All**) palladates with nucleic acids (NAs) such as DNA (natural, poly(dA)-poly(dT) and poly(dG)-poly(dC)), RNA (in double and triple helices) and non-canonical structures of DNA (G-quadruplex and i-motif). Spectrophotometric titrations under different temperature and salt content conditions, viscosimetric experiments, fluorescent intercalator displacement (FID) tests together with theoretical Density Functional Theory (DFT)/Docking calculations are used to enlighten the complicated features of the interaction. The binding occurs in the grooves of the polynucleotides and is dominated by the geometrical features of the NA. A strong affinity for RNA double helix is present, together with interesting binding signatures to G-quadruplex and i-motif. The indenyl moiety plays a role and the binding is tighter (**1-Ind** > **2-All**) for all NA systems. However, it is **2-All** that, interestingly, shows the more striking differences in changing from one NA to another. The formation of covalent adducts and other mechanistic features are also discussed.

1. Introduction

Approximately half of cancer patients undergo chemo-radiotherapy, with most protocols involving still nowadays platinum-based antineoplastic agents where the antitumor function of cisplatin (*cis*-diamminodichloroplatinum(II)) derives from its ability to alter DNA structure [1,2]. To overcome the limitations of platinum-based drugs, recent research has focused on developing novel antitumor agents containing metals other than platinum. Palladium is one such metal of interest because of its coordination chemistry similarities with platinum. However, cis-palladium (*cis*-diamminodichloropalladium(II)) lacks antitumor activity since the hydrolysis of leaving groups occurs at a rate approximately 10^5 times faster than that of platinum analogues, resulting in rapid dissociation in solution [3]. This generates highly reactive species unable to reach the desired pharmacological targets. To develop a palladium-based antitumor drug, it is therefore necessary to stabilize the compound using a strongly coordinating ligand [4]. If the latter is relatively stable, the drug can retain its structure in vivo long enough to act. An important advancement in Pd(II) compound research involves the use of chelating ligands, which can even prevent potential *cis-trans* isomerism. Over the years, several palladium complexes with antitumor properties have been developed. One of the earliest was *trans*-[$PdCl_2$(2-diethyl-2-quinolylmethylphosphonate)], synthesized in 1991 [5]. It was tested on tumour cell lines, including human epidermoid carcinoma and leukaemia. Results demonstrated significant cytotoxic activity comparable to cisplatin, measured through IC_{50} values (concentration needed to inhibit 50 % of tumour cell growth). These findings prove the compound's potential as an antitumor agent, interfering with

Abbreviations: c-myc, G-quadruplex DNA – antiparallel form; CTA-22, G-quadruplex DNA – parallel form; dA, deoxyadenine nucleotide; dC, deoxycytidine nucleotide; dG, deoxyguanine nucleotide; dT, deoxythymine nucleotide; DFT, density functional theory; DMF, dimethylformamide; EB, ethidium bromide; FID, fluorescent intercalator displacement; G4, G-quadruplex; LiCac, lithium cacodylate; NA, nucleic acid; NaCac, sodium cacodylate; NHC, N-heterocyclic carbene; rA, riboadenine nucleotide; rU, ribouracyl nucleotide; Tel-23, G-quadruplex DNA – hybrid form.

☆ This article is part of a Special issue entitled: 'ISMEC24' published in Journal of Inorganic Biochemistry.

* Corresponding author.
E-mail address: tarita.biver@unipi.it (T. Biver).

https://doi.org/10.1016/j.jinorgbio.2025.112978
Received 27 March 2025; Received in revised form 4 June 2025; Accepted 17 June 2025
Available online 18 June 2025

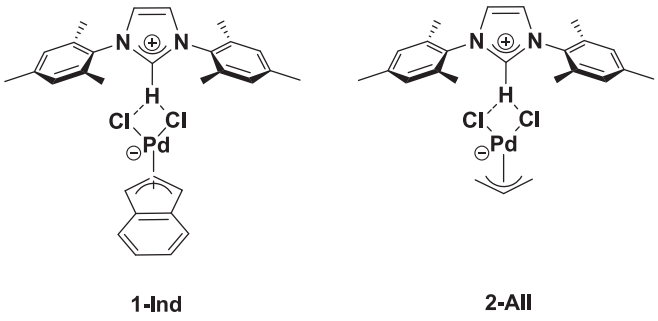

Fig. 1. Molecular structures of the Pd(II) complexes studied in this work.

cellular mechanisms that regulate proliferation. Similarly to what happens with platinum, a key aspect of palladium complex activity lies in its interaction with nucleic acids (NA). At neutral pH, the complex coordinatively binds to nucleic acid bases, inducing significant structural alterations. At acidic pH, interaction increases as the ligand protonates, engaging NAs differently, primarily through electrostatic interactions, while the palladium centre forms a covalent bond. This pH-dependent reactivity may enhance selectivity toward cancer cells, which typically exhibit a slightly acidic microenvironment [6]. Following the development of this first palladium-based antitumor complex, further studies focused on structures with nitrogen-based ligands, leading to the synthesis of [PdCl(ethylenediamine)(8-hydroxyquinoline)] [7]. This complex displayed a significant affinity for natural DNA, intercalating between nucleic acid bases (preferentially guanine-cytosine pairs) and inhibiting cellular replication processes. While promising, these complexes still exhibited greater lability compared to their platinum counterparts, compromising cellular activity. The structure evolved with the substitution of ethylenediamine by cyclohexane-diamine, yielding Pd(II)(1,2-diamino cyclohexane)(dimethylbarbiturate). The addition of strongly chelating and rigid ligands increased the complex's stability in cellular environments, enhancing cytotoxic activity and reducing IC_{50} values [8]. This complex proved effective against animal sarcoma and leukaemia cell lines [9]. Subsequent developments introduced palladium complexes with innovative ligands, such as phosphine ligands, which demonstrated improved cytotoxic activities. These compounds act similarly to platinum-based drugs by intercalating DNA, inhibiting replication, and promoting cell death but exhibit different binding kinetics, allowing greater selectivity toward tumour cells. Among them, [$PdCl_2$(1,1′-bis(diphenylphosphine)ferrocene)] showed superior efficacy and specificity against ovarian and breast cancer cell lines [10]. Additionally, this complex inhibits cathepsin B, making it highly effective against metastatic tumours. More generally, palladacycles act not only through covalent DNA binding but also by interfering with mitochondria, inducing apoptosis via reactive oxygen species (ROS) production. Their chemical stability and ability to generate oxidative stress render them ideal candidates for addressing tumours resistant to traditional treatments. The introduction of *N*-heterocyclic carbene (NHC) ligands further revolutionized palladium complex chemistry: recent studies on [$Pd(NHC)_2(Cl)_2$] complexes have demonstrated promising activity against triple-negative breast cancer, one of the most challenging types to treat [11]. These compounds combine noncovalent DNA binding with the induction of oxidative stress, enhancing therapeutic efficacy while minimizing side effects. Building on these findings, some of us synthesized and characterized a series of new palladium complexes through mechanochemical synthesis, achieving solvent-free high-yield reactions [12]. These complexes showed significant cytotoxicity against ovarian cancer cell lines, with IC_{50} values comparable to or lower than cisplatin. Promising activity against high-grade serous ovarian cancer models further supports their potential against this form of neoplasia. However, the details of their mode of action still need to be explored. In this work, two palladate complexes among those synthesised in [12] were selected to undergo a detailed mechanistic study of their interaction with NAs to unveil some possible routes for their cellular activity (Fig. 1); the major focus is on the indenyl complex **1-Ind**, whereas the allyl counterpart (**2-All**) is used for comparison and to enlighten the possible role of an additonal aromatic residue.

Table 1
Oligonucleotide sequences for the DNA G-quadruplexes (G4) and i-motif used in this work.

Name	Sequence	Morphology
Tel-23	TAG GGT TAG GGT TAG GGT TAG GG	Hybrid
CTA22	AGG GCT AGG GCT AGG GCT AGG G	Parallel
c-myc	TGA GGG TGG GTA GGG TGG GTA A	Anti-parallel
i-motif	CCC TTT CCC TTT CCC TTT CCC TTT	

As NAs, natural DNA (calf thymus), double and triple-stranded RNAs (poly(*rA*)poly(rU) and poly(rA)2poly(rU)) and peculiar oligonucleotide geometries of biomedical interest (G-quadruplexes of different topologies and i-motif) were considered. The results obtained not only indicate the possible preferred targets for these peculiar palladium complexes but more generally offer some structure-reactivity tips. Since the above-mentioned compounds have shown significant cellular activity and are therefore candidates as chemotherapy drugs, this study will lead to a more in-depth knowledge of their mechanisms of action and, possibly, pave the way for further improvements of this interesting class of drugs.

2. Materials and methods

2.1. Materials

The palladium complexes **1-Ind** (MW = 597.92 g/mol) and **2-All** (MW = 523.84 g/mol), in crystalline form, were stored at 4 °C. Stock solutions (ca. 1.0×10^{-3} M) were prepared by dissolving known quantities of the complexes in 1.0 mL of dimethylformamide (DMF). Diluted solutions were obtained by mixing 10 or 20 μL of stock solution with 1 mL of buffer (typically 0.01 M sodium cacodylate (NaCac) and 0.1 M sodium chloride (NaCl) pH 7.0 – see more details below), ensuring negligible DMF final concentration (<2 %). Note that preliminary UV–vis tests with DMSO indicated low stability in this solvent, leading to the choice of DMF. The DNA samples included calf thymus DNA (CT-DNA, Merck) and synthetic polynucleotides (poly(dA)·poly(dT) and poly(dG)·poly(dC), Merck). Their stock solutions were prepared by dissolving lyophilized sodium salts in ultrapure water. CT-DNA solutions underwent sonication to reduce chain length to ca. 500 base pairs. The exact concentrations, expressed in base pairs, were verified via spectrophotometry at 260 nm using molar absorption coefficients (ε) 13,200 cm^{-1} M^{-1} for CT-DNA and poly(dA)·poly(dT), 14,800 cm^{-1} M^{-1} for poly(dG)·poly(dC) [13–15]. Stock solutions were stored at −20 °C and, once thawed, at 4 °C. Synthetic RNA samples included single-stranded poly(rU) and double-stranded poly(rA)·poly(rU) as sodium salts (Merck). Stock solutions were spectrophotometrically characterized using ε values of 8900 cm^{-1} M^{-1} and 14,900 cm^{-1} M^{-1} at 260 nm, respectively [15]. Triple-helical RNA, poly(rA)·2poly(rU), was prepared by annealing equimolar mixtures of the components overnight. Oligonucleotides for G-quadruplex (Tel23, CTA22, c-myc) and i-motif studies were purchased from Metabion; the exact sequences are provided in Table 1. Stock solutions (ca. 1.0×10^{-4} M) were prepared by dissolving oligonucleotides in G4 or i-motif buffers (see below). For annealing, samples were heated at 90 °C for 10 min, cooled overnight, and diluted appropriately for experiments.

Ethidium bromide solid (EB, purity >99 %, Merck) was used to prepare stock solutions by dissolving known amounts of solid in the buffer. The concentrations were verified spectrophotometrically (λ = 480 nm, ε = 5600 M^{-1} cm^{-1}) [16]. Buffers used included 0.01 M sodium cacodylate (NaCac) and 0.1 M sodium chloride (NaCl). For ionic

strength variation studies, buffers with NaCac (0.01 M) and varying NaCl concentrations (0 M to 1.0 M) were prepared. G-quadruplex (G4) interaction studies utilized 2.5 mM lithium cacodylate (LiCac) and 0.1 M potassium chloride (KCl), pH 7.0. I-motif studies employed both the G4 buffer and 50 mM NaCac, pH 5.5.

2.2. Methods – experimental

For UV–Vis spectroscopy we used a Perkin-Elmer Lambda 650 spectrophotometer with double-beam functionality. Absorbance measurements were performed at controlled temperatures (±0.1 °C, Thermo Haake® refrigerated circulator) using quartz cuvettes (1.0 cm path length). DNA and RNA titrations involved incremental addition of polynucleotides to the complex in buffer, with absorbance recorded for analysis. Fluorescence measurements were performed using a Perkin-Elmer LS55 spectrofluorometer equipped with a xenon lamp source. Semi-micro quartz cuvettes (1.0 cm path length in excitation, 0.2 cm in emission) were used. Titrations of ethidium bromide (EB) displacement were conducted under thermostated conditions (±0.1 °C); here, a blank test was performed, to be sure that the change in fluorescence was not due to dilution effects or the presence of DMF. Any type of titration was repeated at least three times; any number shown in the text is mean ± standard deviation.

The binding constants were evaluated using the HypSpec® program from the Hyperquad suite (http://www.hyperquad.co.uk/), which processes UV/visible, infrared, Raman, luminescence and fluorescence data over a whole wavelength range, subject to the single requirement that the spectral intensity of each chemical species should be proportional to the concentration of that species in solution. A "model" defines the chemical species present in the solutions. The concentration of the species at equilibrium and the equilibrium constants are evaluated thanks to a procedure that uses a least-square approach on matrices of non-linear equations of mass balance [17].

Viscosity measurements were performed using a Cannon-Ubbelohde semi-micro viscometer. Solutions were equilibrated at 25.0 °C (±0.1 °C, Thermo Haake® refrigerated circulator) for 15 min before measurements. The relative viscosity (η_{rel}) was calculated using the flow times for the solvent (t_0), the polynucleotide alone (t_P), and the NA/complex mixtures (t) as $\eta_{rel} = \eta/\eta_0 = \eta_{NA/complex}/\eta_{NA} = (t - t_0)/(t_P - t_0)$. The relative viscosity/contour-length relationship is of the form $L/L_0 = (\eta/\eta_0)^{1/3}$ [18]. The flow times were recorded at least six times, any number shown in the text is mean ± standard deviation.

2.3. Methods – theoretical calculations

The structure of complex **1-Ind** was obtained by full geometry optimization. The BLYP functional was used, in combination with a Slater triple zeta quality basis set with two polarization functions [19,20]. The small core approximation was employed and scalar relativistic effects were included using the ZORA approximation [21]. This level of theory is denoted ZORA-BLYP/TZ2P and gives accurate results for compounds with heavy nuclei [22–28]. The DFT calculations were performed using ADF2019 [29,30]. Hirshfeld partial charges computed at the ZORA-BLYP/TZ2P level were employed in the docking simulation. The DNA blind docking studies were carried out using the AutoDock Vina 1.1.1 program [31], using the crystallographic structures from the Protein Data Bank (PDB), according to previous studies [32–35]. The targets included DNA (3FT6), G-quadruplexes (2JSM, 1XAV and 2KM3), i-DNA (7O5E) and poly(*rA*)poly(rU) section of RNA (1AL5). The NAs were prepared using the Chimera 1.8 software, removing water, ions, and other unnecessary molecules [36]. Since AutoDock does not recognize the Pd atom, it was replaced by Zn. In the Pd complex, the H···Cl interactions were treated as covalent bonds, and the H atom from the imidazole moiety was substituted with a C atom to create a bond model capable of rotating during the docking simulations. An exhaustiveness of 50 was used, and the grid boxes were positioned on the center of macromolecules (3FT6: −0.739 × 17.255 × 45.638, 25 × 25 × 15 Å; 2JSM: −0.106 × −0.033 × −1.992, 35 × 35 × 35 Å; 1XAV: −0.049 × 1.228 × 0.970, 35 × 35 × 35 Å; 2KM3: 0.023 × 0.045 × −0.072, 35 × 35 × 35 Å; 7O5E: 41.934 × 51.629 × 49.161, 50 × 50 × 50 Å; 1AL5: −0.509 × −0.058 × 2.514, 25 × 40 × 40 Å). The redocking for the DNA PDB ID 3FT6 yielded an acceptable root mean square deviation (RMSD) of 2.5 Å. For the molecular docking with the NA:metal adducts, the firstly docked 1-Ind complex was treated as a component of the macromolecular target, and a blind docking simulation was run. As a model of the binding pose, the ligand conformers with the lowest predicted binding free energy (ΔG, kcal/mol) were selected and analysed using Discovery Studio Visualizer (DSV) software.

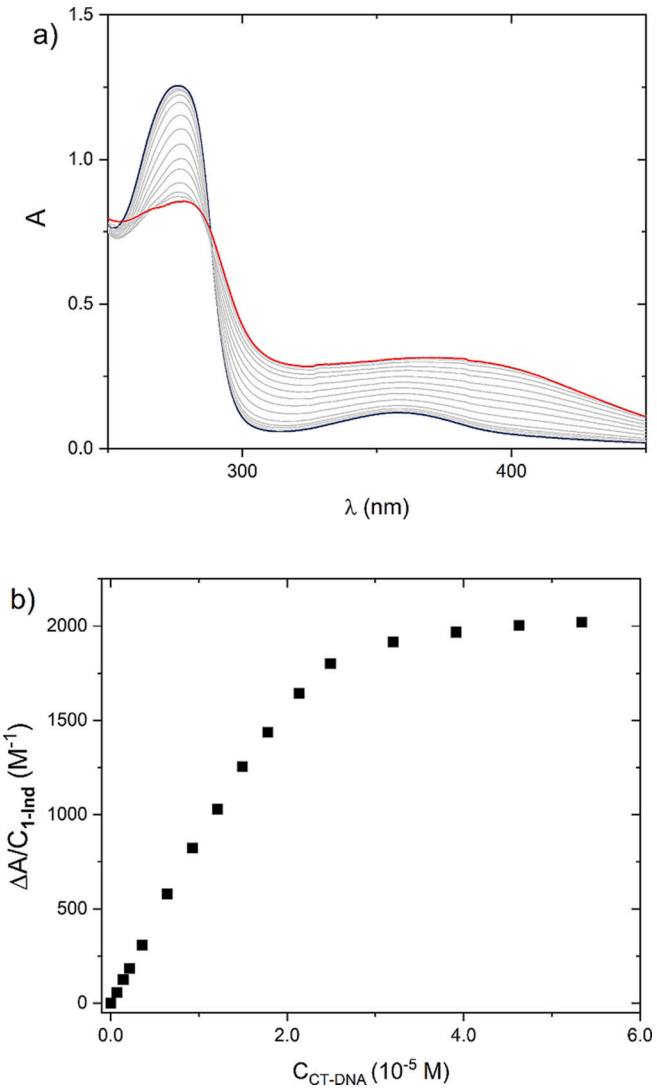

Fig. 2. (a) Titration of **1-Ind** with CT-DNA at 25.0 °C. $C_{1\text{-Ind}} = 7.03 \times 10^{-5}$ M, $C_{CT\text{-DNA}} = 0$ M (blue) to 5.34×10^{-5} M (red), NaCl 0.1 M, NaCac 0.01 M, pH 7.0, DMF 1 % *v*/v; (b) relevant binding isotherm at λ = 358 nm. (For interpretation of the references to colour in this figure legend, the reader is referred to the web version of this article.)

3. Results

3.1. Characterization in solution

Solubility tests on the palladium complexes **1-Ind** and **2-All** revealed that neither could be solubilized in the aqueous buffer. Thus, the complexes were first dissolved in DMF to prepare stock solutions (ca. 8 mM)

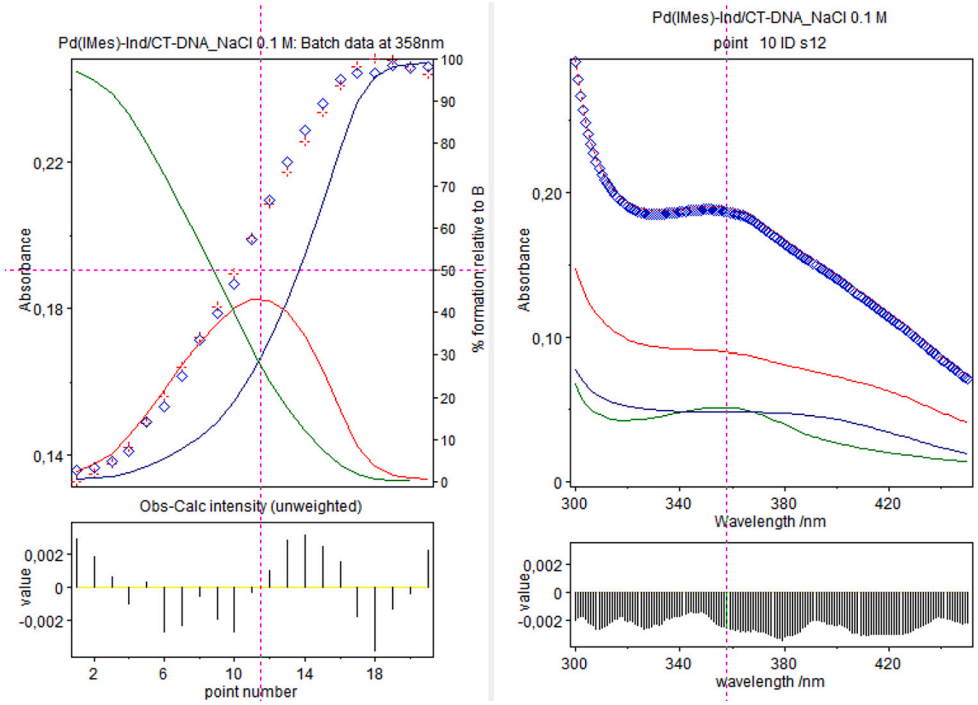

Fig. 3. HypSpec analysis of complex **1-Ind** (D) absorption changes upon CT-DNA (P) addition under a 1:1 + 1:2 NA:metal complex model; blue diamond = experimental, red cross = calculated. Left: titration curve at 358 nm and species distribution (green = free complex, blue = PD, red = PD_2). Right: spectra deconvolution. Lower panels are the residuals. (For interpretation of the references to colour in this figure legend, the reader is referred to the web version of this article.)

and subsequently diluted in the aqueous buffer (DMF < 2 %). Stability was assessed spectrophotometrically immediately after diluting the stock solution in the buffer. For complex **1-Ind**, absorption spectra were recorded every 10 min over one hour at 25.0 °C, 50.0 °C, and 60.0 °C. At 25.0 °C and 50.0 °C, signal variation over time was less than 3 % (Fig. S1). However, at 60.0 °C, the signal decreased by 19 % within 90 min (Fig. S2), indicating instability above 50.0 °C. This precluded high-temperature studies such as DNA melting experiments. For **2-All**, stability was confirmed at 25.0 °C using the same method (Fig. S3). The proportionality between absorbance and concentration was evaluated for both complexes from 1.0×10^{-5} M to ca. 1.0×10^{-3} M. Absorption spectra were recorded following incremental additions of the complexes to aqueous buffer solutions. The results confirmed that both complexes **1-Ind** (Figs. S4) and **2-All** (Figs. S5) adhered to Lambert-Beer's law, maintaining linearity between absorbance and concentration.

3.2. *DNA polynucleotides: Interaction with natural DNA*

The interaction with natural DNA (calf thymus DNA, CT-DNA) was evaluated through spectrophotometric titrations of solutions containing the palladium complexes under study. Titrations were conducted by adding the polynucleotide to both the sample cuvette (containing the complex) and the reference cuvette (containing only the buffer). This "double addition" method eliminates the contribution of DNA absorbance at λ = 260 nm, which overlaps with signals from other species (free complex and adduct). The double addition of DNA also to the reference cuvette highlights isosbestic points, confirming adduct formation between the complexes and the polynucleotide. Graphing the normalized signal variation at specific wavelengths versus DNA concentration produces a binding isotherm, a useful tool to monitor the titration progression and endpoint. Fig. 2 displays the titration spectra of **1-Ind** with CT-DNA at 25.0 °C. Increasing CT-DNA concentrations results in signal increases between 280 nm and 450 nm, particularly above 320 nm, where DNA does not contribute to the overall signal. This confirms the interaction between the palladium complex and the polynucleotide. Note that, in these experiments, the equilibration time was checked and found to be very fast.

Equilibrium constants were determined using HypSpec® software (see Methods). Pre-tests in the search for a correct model indicated that a simple 1:1 molecule-to-base pair interaction model was insufficient to describe the experimental data (Fig. S6). Further testing revealed that a model incorporating two equilibria (1:1 and 1:2) was required. Fig. 3 illustrates the results generated under this model where both the reaction $P + D \rightleftarrows PD$ and $PD + D \rightleftarrows PD_2$ are considered, where P is the polynucleotide (in base pairs units) and D is the metal complex (dye, drug). Fig. 4 shows the numerical values for the equilibrium constants of these two reactions.

The polyanionic nature of DNA due to its negatively charged phosphate groups makes it highly sensitive to ionic strength. The equilibrium constant (K) dependence on ionic strength was analysed for the **1-Ind**/CT-DNA system by varying NaCl concentrations (0.02 M to 0.3 M) while keeping NaCac (0.01 M), pH (7.0), and temperature (25.0 °C) constant. Table S1 and Fig. 4 collect the results.

The central plateau in the equilibrium constants values between 0.04 M and 0.15 M NaCl agrees with neutral complex-DNA interactions, these being unaffected by sodium ion concentration and involving no release of counterions. Beyond this range, a decrease in affinity is observed. Studies at 0 M or 0.5 M NaCl concentrations have proven impossible since the absorption spectrum of the complex varies greatly. For example, at 0 M the spectrum no longer presents the characteristic band with the maximum at 358 nm. This suggests that, under extreme salt conditions, the complex **1-Ind** is not stable. At high ionic strength, the complex can undergo dissociation by exchange of ligands. At low ionic strength, the complex may suffer hydrolysis or structural rearrangements because the reduced electrostatic shielding increases the internal tensions between the protonated carbene and the chlorides. Also, the reduced ionic strength facilitates conformational transitions of the helix and changes in DNA geometry may reduce the accessibility of binding sites for metal complexes. Overall, these tests indicate: (i) that the **1-Ind** complex is perceived by the NA as an overall neutral entity;

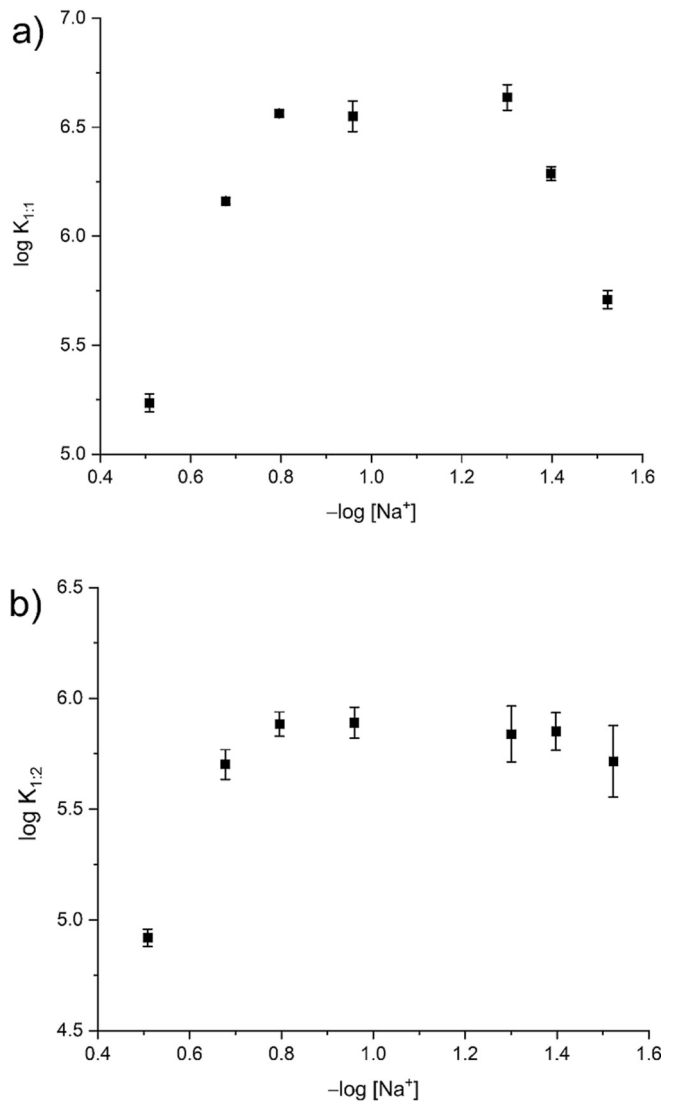

Fig. 4. Dependence of the 1:1 (a) and 1:2 (b) binding constants for the **1-Ind**/CT-DNA system on the NaCl content of the medium. C_{NaCl} = 0.02–0.3 M, C_{NaCac} 0.01 mM, pH 7.0, T = 25.0 °C.

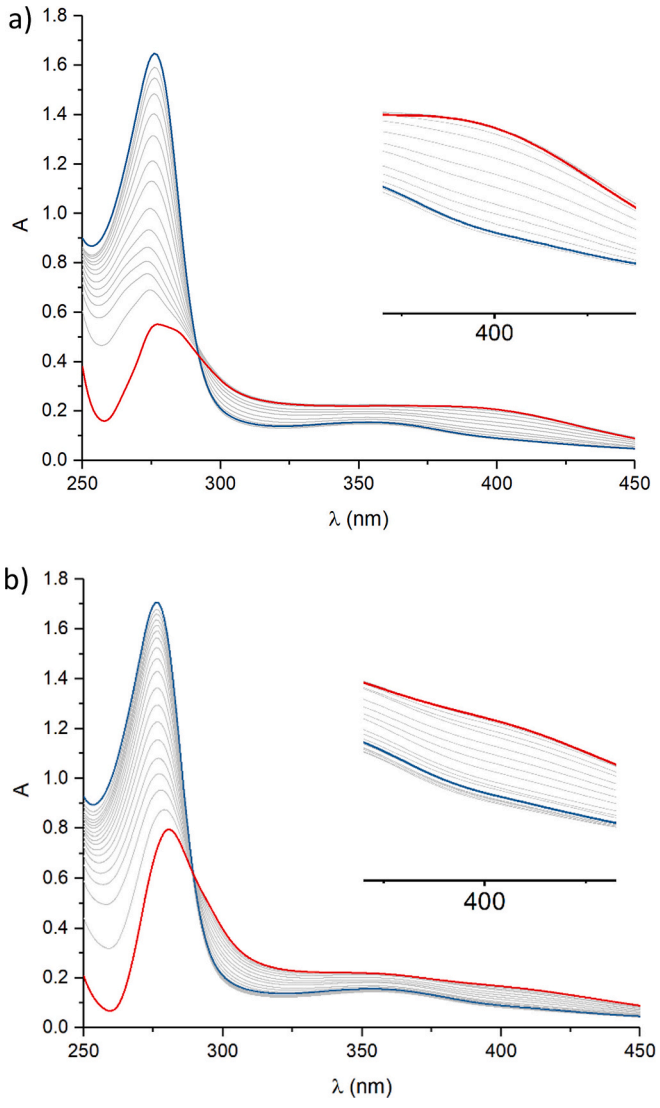

Fig. 5. Titrations of complex **1-Ind** with poly(dA)·poly(dT) (a) and poly(dG)·poly(dC) (b). $C_{\mathbf{1\text{-}Ind}} = 8.36 \times 10^{-5}$ M, NaCl 0.1 M, NaCac 0.01 M, pH 7.0, DMF 1 % v/v, T = 25.0 °C. (a) $C_{poly(dA)\cdot poly(dT)}$ = 0 M (blue) to 7.79×10^{-5} M (red), (b) $C_{poly(dG)\cdot poly(dC)}$ = 0 M (blue) to 1.65×10^{-4} M (red). (For interpretation of the references to colour in this figure legend, the reader is referred to the web version of this article.)

(ii) the stability within the physiological ionic strength window.

As for the thermodynamic aspects, the analysis was further extended by performing **1-Ind**/CT-DNA titrations at different temperatures, at constant ionic strength and pH (NaCl 0.10 M; NaCac 0.01 M; pH 7.0). Figs. S7-S9 show examples of spectra and relevant binding isotherms: variations in the curvature of the latter are evident. For all temperatures, the experimental data were best described by the already cited 1:1 + 1:2 equilibrium model. Table S2 summarizes the values obtained for each of the investigated temperatures. These were used to construct van't Hoff plots (Fig. S10). From these data, the following thermodynamic parameters can be extracted: for 1:1 process $\Delta H = 35 \pm 5$ kJ/mol, $\Delta S = 244 \pm 24$ J/mol K, $-T\Delta S = -73 \pm 5$ kJ/mol; for 1:2 process $\Delta H = -4 \pm 4$ kJ/mol, $\Delta S = 94 \pm 13$ J/mol K, $-T\Delta S = -28 \pm 5$ kJ/mol. These results indicate an entropy-favoured and enthalpy-disfavoured interaction. The 1:1 thermodynamic signature is inconsistent with the intercalative behaviour (highly negative ΔH) but aligns with a groove/external interaction between the complex and the polynucleotide [37]. These latter interactions are driven by an entropy increase due to the release of water molecules from the DNA grooves and/or first coordination sphere. In the case of the 1:2 adduct, $\Delta H \approx 0$ agrees with some electrostatic stacking.

A comparative test for complex **2-All**/CT-DNA was also done by a double-addition titration at 25.0 °C (Fig. S11). Differently from complex **1-Ind**/CT-DNA, the HypSpec analysis showed that **2-All**/CT-DNA data are well described by a 1:1 model. The equilibrium constant was $K_{1:1} = 1.29 \times 10^4$, significantly lower than that of **1-Ind**/CT-DNA.

3.3. *DNA polynucleotides: Interaction with synthetic AT/GC DNAs*

Spectrophotometric titrations were done to study the interaction of the palladium complexes with synthetic DNA polynucleotides composed exclusively of adenine-thymine (poly(dA)·poly(dT)) or guanine-cytosine (poly(dG)·poly(dC)) base pairs, aimed to determine any preferential binding to specific base pairs or helix geometries. The titrations were performed at 25.0 °C as described in the previous sections. Figs. 5 and 6 show the results for complexes **1-Ind** and **2-All**, respectively.

While the titrations of complex **1-Ind** with both synthetic polynucleotides seem similar, some differences appear in the 380–450 nm wavelength range (inserts in Fig. 5). Specifically, poly(dA)·poly(dT) titrations show a more pronounced absorption band around 400 nm,

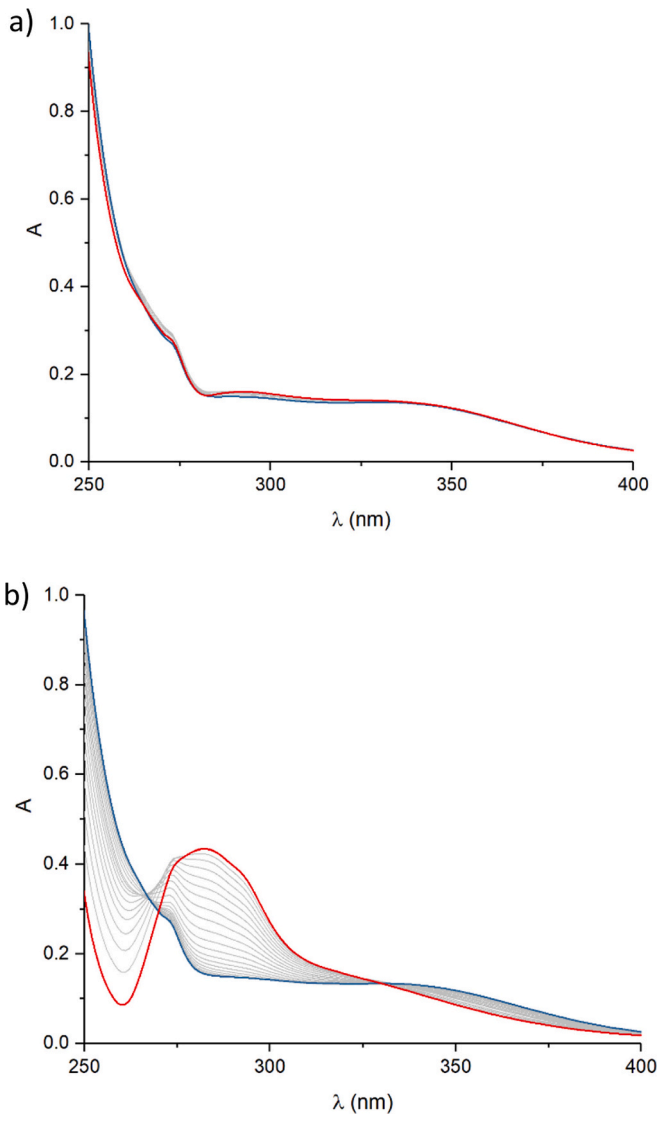

Fig. 6. Titrations of complex **2-All** with poly(dA)·poly(dT) (a) and poly(dG)·poly(dC) (b). $C_{\mathbf{2\text{-}All}} = 1.91 \times 10^{-4}$ M, NaCl 0.1 M, NaCac 0.01 M, pH 7.0, DMF 1 % v/v, T = 25.0 °C. (a) $C_{poly(dA)\cdot poly(dT)} = 0$ M (blue) to 2.92×10^{-5} M (red), (b) $C_{poly(dG)\cdot poly(dC)} = 0$ M (blue) to 2.16×10^{-4} M (red). (For interpretation of the references to colour in this figure legend, the reader is referred to the web version of this article.)

Table 2
Comparison of binding constant values ($K_{1:1}$) for the palladium complexes with synthetic DNA polynucleotides at 25.0 °C in NaCl 0.1 M, NaCac 0.01 M, pH 7.0 buffer. $K_{1:2}$ exists only for the complex **1-Ind**/poly(dA)·poly(dT) system where $K_{1:2} = (6.8 \pm 0.6) \times 10^4$.

	$K_{1:1}$ ($\times 10^4$)		
Complex	**poly(dA)·poly(dT)**	**poly(dG)·poly(dC)**	**Selectivity GC/AT**
1-Ind	4.2 ± 0.4	15.4 ± 1.1	3.7
2-All	0.07 ± 0.01	2.7 ± 0.2	39

associated with higher stoichiometry adducts (e.g. 1:2). Indeed, the **1-Ind**/poly(dA)·poly(dT) system required a 1:1 + 1:2 equilibrium model for accurate representation (Fig. S12) as the simpler 1:1 model is not able to satisfactorily reproduce the experimental trend (Fig. S13); the relevant data interpolation confirms the contribution of the 1:2 species to the signal at ca. 400 nm (Fig. S12). In contrast, the poly(dG)·poly(dC) titration fit well with a simple 1:1 model (Fig. S14). Thus, steric and geometric factors influence complex-DNA interactions, with varying reactivity toward different base pairs. For the **2-All** complex, the two titrations exhibited stark differences across all wavelengths studied, with spectral variations dramatically reduced in the poly(dA)·poly(dT) case. While both palladium complexes favoured GC pairs, **2-All** exhibited this preference more prominently (Table 2). Given that prior measurements suggested that groove binding is predominant, it seems sound that variations in helix groove geometry and rigidity modulate interaction. The affinity disparity between the two palladium complexes observed with natural polynucleotides remains consistent with the results obtained with the synthetic DNA.

3.4. Adenosine triphosphate (ATP) binding

ATP was also tested, so to highlight how the palladium complexes interact specifically with nitrogenous bases and phosphate groups, without the influence of grooves and base stacking present in NAs (Fig. S15). $K_{1:1}$ values were found to be 8.15×10^3 for the complex **1-Ind** and 6.17×10^3 for the complex **2-All**. These values decrease by factors of 38 and 2, respectively, compared to natural long-chain DNA (CT-DNA). This test highlighted that the influence of the DNA helix and base pairing on interaction strength is relatively high for **1-Ind**, much less for **2-All**. The binding occurs also in the presence of a single nitrogenous base, likely through π–π stacking interactions, but the lack of an extended groove precludes other interaction modes. The substantial reduction in binding affinity for **1-Ind** suggests that, in this case, the presence of a long-chain DNA with its grooves is a discriminating factor. This finding may have two (non mutually-exclusive) explanations: (i) some partial intercalation/anchoring involving the indenyl moiety; (ii) some favourable groove binding by the indenyl group. Docking data (see paragraph 3.9) suggest that option (ii) plays a major role.

3.5. RNA polynucleotides: Interaction with poly(rA)•poly(rU) and poly(rA)•2poly(rU)

Long RNA polynucleotides are generally less used in the kind of experiments we are presenting in this work. However, this gap needs to be filled considering the extreme importance of RNAs. We thus considered the interactions of the palladium complexes with both double- and triple-helical RNA by a procedure that mirrored that used with DNA. Starting from the RNA double helix, we titrated complex **1-Ind** with poly(rA)•poly(rU) at various temperatures (18.0–50.0 °C; NaCl 0.10 M; NaCac 0.01 M; pH 7.0). A comparative analysis with the complex **2-All** was done by performing three replicates of a microtitration at 25.0 °C. Figs. S16-S23 show examples of these data. The titrations were as usual analysed using HypSpec®: for double-helical RNA, a 1:1 model adequately described the experimental response in all cases (Fig. S24). Table S3 collects the binding constant parameters and Fig. S10 shows the relevant van't Hoff plot. As with DNA, thermodynamic interaction values for **1-Ind**/poly(rA)•poly(rU) were estimated: $\Delta H = 16 \pm 2$ kJ/mol, $\Delta S = 191 \pm 4$ J,/mol K and $-T\Delta S = -57 \pm 2$ kJ/mol. Again, the entropy contribution is predominant, suggesting an external/groove interaction. The equilibrium constant of **2-All**/poly(rA)•poly(rU) was $K_{1:1} = 1.16 \times 10^4$, i.e. three orders of magnitude smaller compared to the adduct formation constant for **1-Ind**/poly(rA)•poly(rU) at the same temperature. Interestingly, equilibrium constants for interactions with double-helical RNA were higher than those for CT-DNA ($K_{1:1} = (1.4 \pm 0.2) \times 10^7$ for **1-Ind**/poly(rA)•poly(rU); $K_{1:1} = (3.1 \pm 0.2) \times 10^6$ for **1-Ind**/CT-DNA at 25.0 °C). RNA typically adopts an A-type double-helix conformation, whereas DNA primarily adopts a B-type conformation. These conformational differences may influence the accessibility and reactivity of groove binding sites for metal complexes.

The tests above are repeated with synthetic triple-stranded RNA poly(rA)•2poly(rU). Figs. S25-S31 show examples of these data. In the case of triple helix RNA, the 1:1 model is again sufficient to describe the spectral variations. The presence of the third strand in the groove

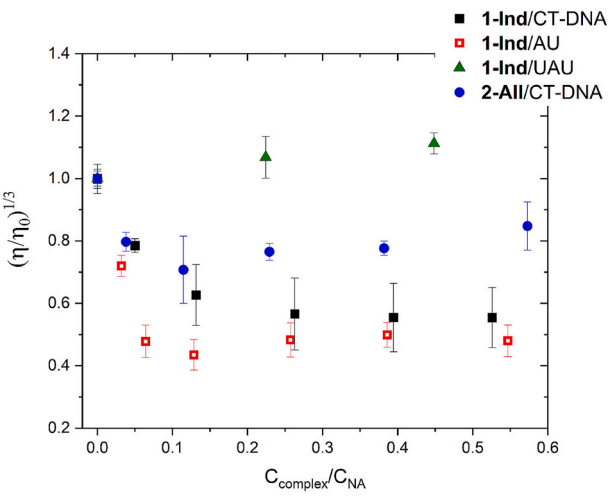

Fig. 7. Relative viscosity plots as a function of the ratio $C_{complex}/C_{NA}$. $C_{CTDNA} = 9.75 \times 10^{-5}$ M, $C_{poly(rA)\bullet poly(rU)} = 8.67 \times 10^{-5}$ M, $C_{poly(rA)\bullet 2poly(rU)} = 5.97 \times 10^{-5}$ M, NaCl 0.1 M, NaCac 0.01 M, pH 7.0, DMF < 1 % *v*/v, $T = 25.0$ °C.

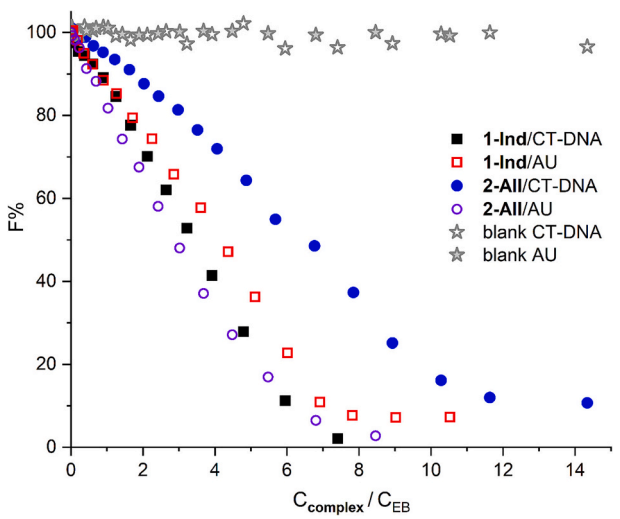

Fig. 8. Change in fluorescence percentage (F% = 100 × F/F_0, F dilution corrected) in FID experiments with EB; a blank test (addition of DMF only) is also shown. For CT-DNA: $C_{CTDNA} = 6.21 \times 10^{-4}$ M, $C_{EB} = 1.11 \times 10^{-4}$ M; for poly(*rA*)poly(rU): $C_{poly(rA)\bullet poly(rU)} = 3.25 \times 10^{-4}$ M, $C_{EB} = 7.90 \times 10^{-5}$ M. For both NAs: $C_{\mathbf{1\text{-}Ind}} = 0$–$6.16 \times 10^{-4}$ M, $C_{\mathbf{2\text{-}All}} = 0$–$1.59 \times 10^{-3}$ M, NaCl 0.1 M, NaCac 0.01 M, pH 7.0, $\lambda_{ex} = 520$ nm, $\lambda_{em} = 595$ nm, DMF = 0–10 % *v*/v, $T = 25.0$ °C.

disturbs the interaction with the palladium complex, turning in equilibrium constants which are 3 orders of magnitude lower than the relative constants with double-stranded RNA ($K_{1:1} = (4.4 \pm 0.3) \times 10^4$ for **1-Ind**/poly(rA)•2poly(rU) at 25.0 °C, Table S4) The relevant van't Hoff plot is shown in Fig. S10; for triplex RNA the binding is again entropically driven, being $\Delta H = 80 \pm 5$ kJ/mol, $\Delta S = 359 \pm 25$ J/mol K and $-T\Delta S = -107 \pm 7$ kJ/mol. Fig. S32 collects and compares at a glance the thermodynamic parameters for the **1-Ind**/CT-DNA, **1-Ind**/poly(rA)•poly(rU) and **1-Ind**/poly(rA)•2poly(rU) systems. For **2-All**/poly(rA)•2poly(rU) (Fig. S33) the equilibrium constant at 25.0 °C, $K_{1:1} = 3.83 \times 10^2$, is approximately two orders of magnitude lower than the result obtained with the indenyl complex. It can again be proposed that, for **1-Ind**, either the indenyl moiety tends to intercalate at least partially between the base pairs of the NAs or that the overall metal complex can adopt a geometry where the indenyl group also allocates in the groove accentuating the complex-NA interaction (see Fig. 9). For both complexes, the preferential site continues to be the groove.

3.6. Viscosity measurements on polynucleotides

The viscometric analysis was performed maintaining the NA concentration constant and different $C_{complex}/C_{NA}$ ratios in the 0 to 0.5 range. Higher ratios led to precipitation phenomena under the relatively high concentrations needed. The results are shown in Fig. 7.

A decreasing viscosity (strand compaction) is associated in the literature with an external (and also sometimes covalent) interaction, whereas its increase suggests intercalation and constancy groove binding [38]. On the other hand, partial intercalation may produce a very limited increase in viscosity, while partial intercalation at two points of the helix (bridging) may cause a helix contraction. In general, these are very complex patterns but viscosity tests remain useful to propose interaction models. For the here analysed systems, with double helices (CT-DNA and poly(rA)•poly(rU)) the viscosity strongly decreases already at low ratios and then stabilises. For RNA the decrease is steeper, following the greater affinity. Excluding bridging intercalations (thermodynamic data), groove binding, possibly also producing a covalent type of interaction and helix roll-up, seems a possible picture. The two systems **2-All**/CT-DNA and **1-Ind**/CT-DNA behave similarly, the latter showing a more pronounced variation following the greater affinity. A different trend is found with triple helical poly(rA)•2poly(rU) where the viscosity increases slightly: the groove is no longer available and the only interaction observed could be linked to a slight intercalation.

3.7. Fluorescent Intercalator displacement (FID) tests

Ethidium bromide (EB) is a very well-known intercalating agent in NAs. When free in an aqueous environment, EB fluorescence is very weak but switches on upon intercalation. EB may thus be used in FID experiments, to test the ability of a molecule to alter its position in the intercalation pocket. The NA is saturated with EB in the first step, and then the palladium complex is added in the cuvette, observing whether or not the addition of the molecule changes the typical response of the intercalated adduct ($\lambda_{ex} = 520$ nm, $\lambda_{em} = 595$ nm) (Fig. S34). Fig. 8 shows how the percentage fluorescence (F% = 100 × F/F_0, F dilution corrected) changes at different $C_{complex}/C_{EB}$ ratios. The dramatic expulsion process for EB indicates that the interaction between complex **1-Ind** and the NA induces a significant structural change of the helix (see the decrease in viscosity). Since strong/full intercalation may be ruled out given previous thermodynamic experiments, we cannot exclude the formation (under these conditions) of a covalent bond between the palladium complexes and NAs. In this context, we have recently studied (via DFT experiments) the reactivity of allyl and indenyl palladates toward nucleophiles, which seems to involve the replacement of one chloride ligand (with the formation of a new bond between palladium and the nucleophile) [39].

3.8. DNA oligos: Interaction with G4s and i-motif

Particular DNA oligos are of high interest as they are found in crucial genetic regions, such as telomeres and promoters of oncogenes, and are involved in the regulation of gene expression and genomic stability. In the spectrophotometric analysis, we chose three types of G4 oligonucleotides: Tel-23 (hybrid form), CTA-22 (parallel form) and c-myc (antiparallel form) (for the exact sequences see the "Materials and Methods" section). Figs. S35-S40 show examples of the absorption spectra collected. Complex **1-Ind** interacts with all the proposed oligonucleotides with 1:1 stoichiometry. The affinities are very similar for all geometries, although slightly lower for c-myc. Unlike the indenyl complex, complex **2-All** does not interact with all the proposed oligonucleotides since there is no binding with c-myc; also, the affinity for CTA22 is significantly lower than that for Tel-23. Concerning the i-motif (Figs. S41-S44) two buffers were taken into account. One is the same used for G4s (KCl 0.1 M, LiCac 2.5 mM, pH 7.0), and the second is 50 mM

Table 3
Binding Constants (1:1 stoichiometry) between complex **1-Ind** or **2-All** and selected non-canonical oligonucleotides at $T = 25.0$ °C. For G-quadruplexes (G4): buffer KCl 0.1 M, LiCac 2.5 mM, pH 7.0, for the i-motif: buffer (1) KCl 0.1 M, LiCac 2.5 mM, pH 7.0, buffer (2) 50 mM NaCac, pH 5.5.

	$K_{1\text{-Ind}}$ ($\times 10^5$)	$K_{2\text{-All}}$ ($\times 10^5$)	Morphology
Tel-23	2.7 ± 0.5	0.27 ± 0.03	G4 - Hybrid
CTA22	3.2 ± 0.7	0.04 ± 0.01	G4 - Parallel
c-myc	2.0 ± 0.1	/	G4 - Antiparallel
i-motif pH 7.0	1.2 ± 0.2	0.27 ± 0.03	Partly folded
i-motif pH 5.5	0.11 ± 0.01	0.46 ± 0.08	Fully folded

NaCac, pH 5.5. Whilst the first one was considered for comparison purposes and to adhere better to physiological conditions, a weakly acidic solvent ensures complete folding. The titrations of **1-Ind** with the i-motif show spectroscopic profiles that are very similar at the two pHs, but the numerical values of the equilibrium constant change: $K_{pH\ 5.5}$ is ca. 10 times smaller than $K_{pH\ 7.0}$ (likely due to more geometrical restrictions in the fully folded form). Oppositely, for **2-All** the two titrations are very different as for the UV–vis signature (probably different adducts are formed) but the equilibrium constants are numerically very similar. Note that all titrations show an increase in absorbance change with increasing NA concentration, except for **2-All** with Tel23, CTA22, and i-motif, which show a decrease. An explanation for this contrasting behaviour is speculated in the Conclusions paragraph. All 1:1 equilibrium constants are reported in Table 3.

3.9. Molecular docking simulations with DNA/RNA

Molecular docking simulations were applied to generate binding models between NAs and complex **1-Ind**. The ligand interactions were thermodynamically favourable, with the predicted binding energies (ΔG, kJ/mol) ranging from −26.4 to −31.4 (Table S5). Complex **1-Ind** presents different binding orientations with the NAs targets, showing mainly hydrophobic and dipole-dipole interactions, as well as Van der Waals contacts (Fig. 9). The mesityl group was responsible for many of the hydrophobic interactions (π-π and alkyl-π) with the nucleobases, and the chloride ligands played an important role in the dipole-dipole interactions with the amino groups from deoxyguanine (dG), deoxycytidine (dC), and deoxyadenosine (dA) nucleotides. In addition, an intramolecular cation-π interaction between the Pd ion and the indenyl moiety was observed. Using the DNA PDB ID 3FT6 as the macromolecule target, which contains a pocket from the co-crystalized proflavine intercalated into the DNA, only a mesityl group from complex **1-Ind** was intercalated between dC1, dG2, dC5, and dG6 residues of DNA (Fig. 9A). In the G-quadruplex human telomeric variant (2KM3), sequence (CTAGGG)n, the indenyl moiety presented π-π T-shaped interaction with dT12 residue (Fig. 9G). In the docking simulation with RNA, focusing on

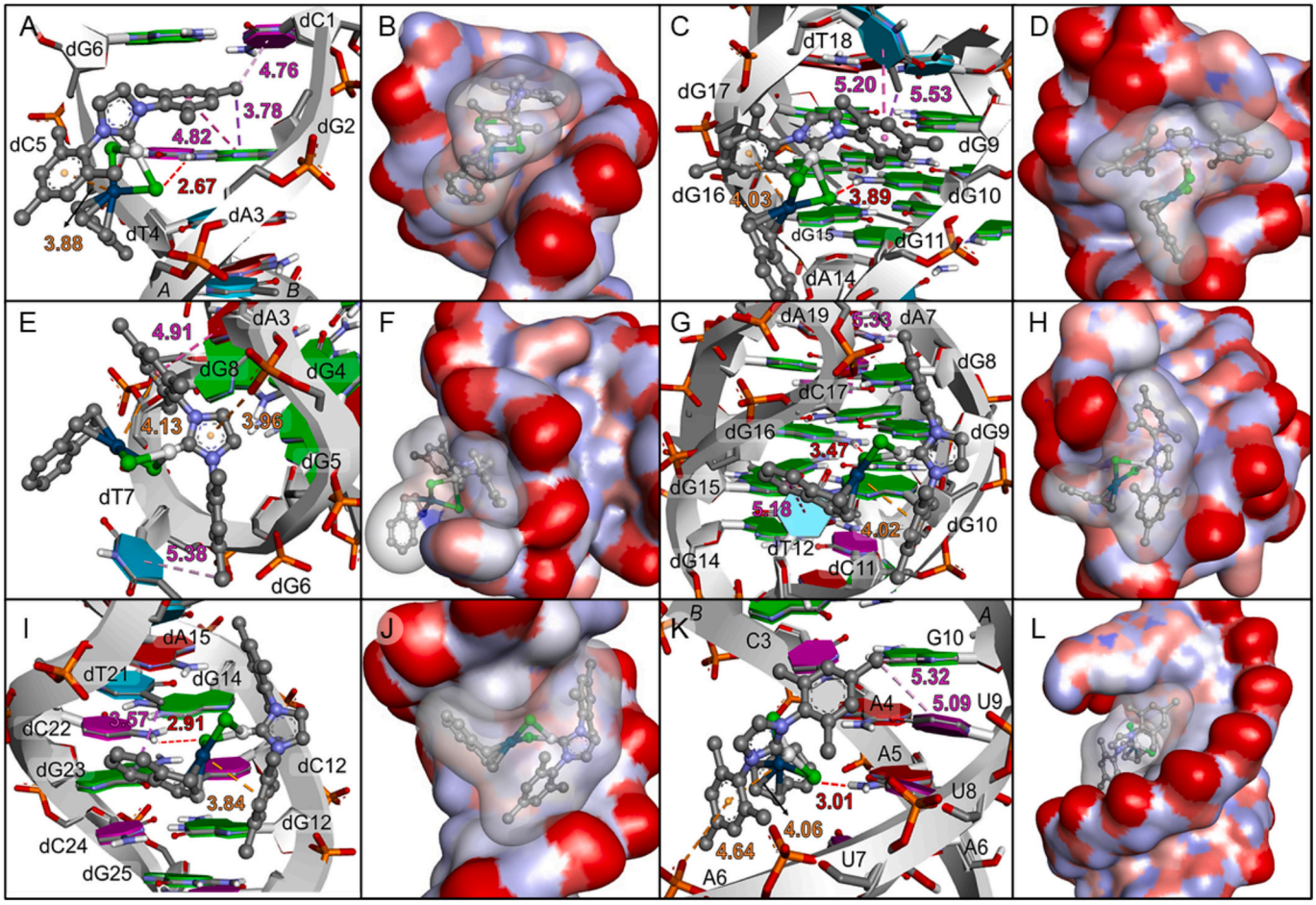

Fig. 9. Binding mode of complex **1-Ind** in the DNA (A–J) and RNA (K–L) target molecules. PDB IDs: (A, B) 3FT6; (C, D) 2JSM; (E, F) 1XAV; (G, H) 2KM3; (I, J) 7O5E; (*K*,*L*) 1AL5. DNA and RNA are represented by backbone arrows and base pair rings. The surface model is coloured by atom charges, and the palladium complex is shown by the ball-and-stick model. Hydrophobic (π-π and alkyl-π), dipole-dipole, and anion/cation-π interactions are represented by purple, red, and orange dashed lines with their respective distances in Å. The DNA rings in red, blue, pink, and green correspond to the nucleotide residues deoxyadenosine (dA), deoxythymidine (dT), deoxycytidine (dC), and deoxyguanosine (dG), respectively (or adenosine (A), uridine (U), cytidine (C), and guanosine (G) in the RNA). (For interpretation of the references to colour in this figure legend, the reader is referred to the web version of this article.)

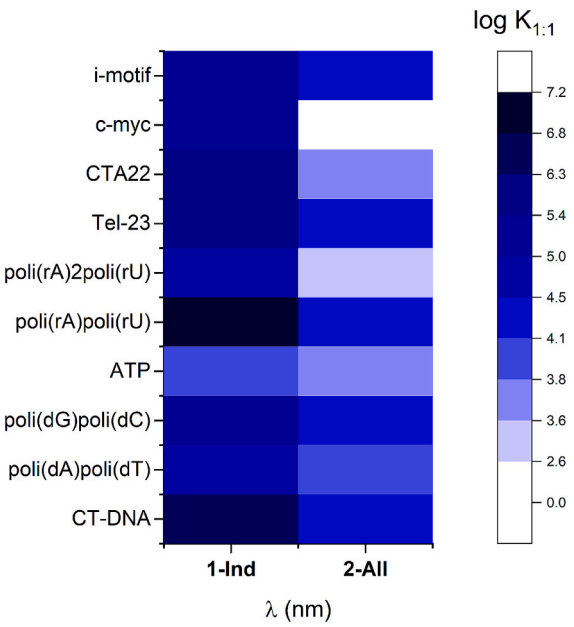

Fig. 10. Comparison of logK values (1:1 binding mode) for the systems analysed in this work; NaCl/KCl 0.1 M, LiCac/NaCac 2.5 mM, pH 7.0, 25.0 °C.

the AAAUUU region (1AL5), the palladium complex binds to the major groove, demonstrating hydrophobic contacts with U9 and G10, and an anion-π interaction with the phosphate moiety of A6 residue. Together, these interactions are important to stabilize the ligand in the NAs binding sites. Note that the more favourable ΔG is found in the case of RNA (Table S5), in agreement with experimental findings.

In addition, to better understand the formation of 1:2 NA:metal complexes, molecular docking simulations were performed using the NA:**1-Ind** adduct as a target (Fig. S45). Considering the potential binding of a second **1-Ind** molecule to the NA:**1-Ind** complex, our models suggest that this binding may occur near the first palladium complex, with favourable binding energies (Table S5) and intermolecular interactions, such as hydrophobic (π–π, alkyl–π) and π–cation interactions. These interactions involve both palladium complexes and the NA targets, contributing to the stabilization of the resulting adducts. In contrast, for RNA, only weak interactions were observed, and no π–cation stacking was detected, indicating that, in this case, the formation of 1:2 complexes is not favourable/relevant. Furthermore, we ran the molecular docking simulations with the individual fragments of **1-Ind**, i.e. the anion $[PdCl_2(\eta^3\text{-indenyl})]^-$ and the cation $[Mes\text{-}Im\text{-}Mes]^+$ (Fig. S46). Although both components bind in a similar region of the **1-Ind** complex (except in the case of the G4 structure PDB ID: 1XAV), the cation generally exhibits more favourable binding energies and interactions than the anion (Table S5). However, the docking results indicate that the binding of the intact **1-Ind** complex is overall more favourable, due to its more negative binding energies and to the great numbers of interactions with the NA targets.

4. Conclusions

We have presented a detailed study of the mechanistic and geometrical factors driving the possible interaction of indenyl and allyl palladate complexes with NAs. It considered both DNA and RNA polynucleotides and DNA non-canonical forms such as G4 and i-motif. Fig. 10 compares at a glance all binding affinities. Here, and in general, 1:1 binding is considered, given that higher stoichiometry was needed only in the cases of **1-Ind**/CT-DNA and **1-Ind**/poly(dA)·poly(dT) and connected to some aggregates.

Complex **1-Ind** has always a higher affinity for NAs compared to complex **2-All**, highlighting the positive contribution of the indenyl moiety. Complex **2-All** showed a weaker binding but, interestingly, a much more selective behaviour (AT vs GC and G4s). Both complexes interact with the NAs according to an entropically favoured groove binding mode. The experiments and docking calculations indicate that the indene residue is mainly placed in the groove and fosters a better geometrical complementarity of the overall metal complex with the external helix. Unfortunately, this aspect is not able to produce high selectivity between different double helix forms. Also, docking studies have shown that some intercalation of the mesityl ligand may instead play a role, hinting at π-π interactions with the nucleobases. It may be speculated that, for **2-All** — lacking from an indenyl/azolium-mesityl synergy— in the presence of the different geometry of the G-tetrad and of the G4 grooves, a different, end-stacked form is prevailing. Interestingly, the born of a favourable but different binding mode increases the possible selectivity of **2-All** for different NAs. The overall picture, as it typically occurs with groove binding, shows the importance of the geometry to drive changes in the interaction mode. Moreover, the well-known reactivity of allyl and indenyl complexes toward nucleophiles — which can involve nucleophilic attack either on the allyl or indenyl ligand or on the metal centre (resulting in the removal of a chloride ligand) — might promote the formation of covalent adducts with NAs, as suggested by the viscosity experiments and fluorescent probe exchange studies.

We strongly believe that this study would be useful in understanding the promising antitumor activity of allyl and indenyl palladates, which will certainly require in-depth studies on other cellular and molecular targets to reconstruct the overall mechanism of action of these potent multitarget metallodrugs.

CRediT authorship contribution statement

Tommaso Giani: Writing – original draft, Validation, Data curation. **Giannantonio Tomasi:** Validation, Data curation. **Pablo A. Nogara:** Methodology, Data curation, Conceptualization. **Laura Orian:** Methodology, Data curation, Conceptualization. **Fabiano Visentin:** Writing – review & editing, Supervision, Conceptualization. **Thomas Scattolin:** Writing – review & editing, Supervision, Conceptualization. **Tarita Biver:** Writing – review & editing, Supervision, Methodology, Data curation, Conceptualization.

Declaration of competing interest

The authors declare that they have no known competing financial interests or personal relationships that could have appeared to influence the work reported in this paper.

Acknowledgements

Funding by the Italian Ministry of University and Research under the PRIN2022 project 2022APCTNA is gratefully acknowledged.

Appendix A. Supplementary data

Supplementary data to this article can be found online at https://doi.org/10.1016/j.jinorgbio.2025.112978.

Data availability

Data will be made available on request.

References

[1] S. Dasari, P. Bernard Tchounwou, Cisplatin in cancer therapy: molecular mechanisms of action, Eur. J. Pharmacol. 740 (2014) 364–378, https://doi.org/10.1016/j.ejphar.2014.07.025.

[2] G.B. Onoa, G. Cervantes, V. Moreno, M.J. Prieto, Study of the interaction of DNA with cisplatin and other Pd(II) and Pt(II) complexes by atomic force microscopy, Nucleic Acids Res. 26 (1998) 1473–1480, https://doi.org/10.1093/nar/26.6.1473.
[3] S.A.-S. Adnan, K. Mika, Platinum group antitumor chemistry: design and development of new anticancer drugs complementary to cisplatin, Curr. Med. Chem. 13 (2006) 1337–1357, https://doi.org/10.2174/092986706776872970.
[4] T. Lazarević, A. Rilak, Ž.D. Bugarčić, Platinum, palladium, gold and ruthenium complexes as anticancer agents: current clinical uses, cytotoxicity studies and future perspectives, Eur. J. Med. Chem. 142 (2017) 8–31, https://doi.org/10.1016/j.ejmech.2017.04.007.
[5] L. Tušek-Božić, I. Matijašić, G. Bocelli, G. Calestani, A. Furlani, V. Scarcia, A. Papaioannou, Preparation, characterization and activity of palladium(II) halide complexes with diethyl 2-quinolylmethylphosphonate (2-dqmp). X-Ray crystal structures of trans-[Pd(2-dqmp)2X2](X = cl or Br), J. Chem. Soc. Dalton Trans. (1991) 195–201, https://doi.org/10.1039/DT9910000195.
[6] Y. Zhang, Y. Liang, Fabrication of folic acid-modified bovine serum albumin cloaked dual-drug loaded hollow mesoporous silica nanoparticles for pH-responsive and targeted delivery of gastric cancer therapy, Heliyon 10 (2024), https://doi.org/10.1016/j.heliyon.2024.e29274.
[7] H. Mansouri-Torshizi, E. Rezaei, F. Kamranfar, M. Heidari Majd, Investigating the apoptosis ability of Ethylenediamine 8-Hydroxyquinolinato palladium (II) complex, Adv. Pharm. Bull. 6 (2016) 449–453, https://doi.org/10.15171/apb.2016.058.
[8] G. Shigeng, J. Tang, D. Zhang, Q. Wang, Z. Chen, L. Weng, Synthesis, structure, and catalytic activity of palladium complexes with new chiral cyclohexane-1,2-based di-NHC-ligands, J. Organomet. Chem. 700 (2012) 223–229, https://doi.org/10.1016/j.jorganchem.2011.12.008.
[9] A.R. Kapdi, I.J.S. Fairlamb, Anti-cancer palladium complexes: a focus on PdX2L2, palladacycles and related complexes, Chem. Soc. Rev. 43 (2014) 4751–4777, https://doi.org/10.1039/C4CS00063C.
[10] C. Bincoletto, I.L.S. Tersariol, C.R. Oliveira, S. Dreher, D.M. Fausto, M.A. Soufen, F. D. Nascimento, A.C.F. Caires, Chiral cyclopalladated complexes derived from N,N-dimethyl-1-phenethylamine with bridging bis(diphenylphosphine)ferrocene ligand as inhibitors of the cathepsin B activity and as antitumoral agents, Bioorg. Med. Chem. 13 (2005) 3047–3055, https://doi.org/10.1016/j.bmc.2005.01.057.
[11] S. Ray, R. Mohan, J.K. Singh, M.K. Samantaray, M.M. Shaikh, D. Panda, P. Ghosh, Anticancer and antimicrobial Metallopharmaceutical agents based on palladium, gold, and silver N-heterocyclic Carbene complexes, J. Am. Chem. Soc. 129 (2007) 15042–15053, https://doi.org/10.1021/ja075889z.
[12] T. Scattolin, I. Pessotto, E. Cavarzerani, V. Canzonieri, L. Orian, N. Demitri, C. Schmidt, A. Casini, E. Bortolamiol, F. Visentin, F. Rizzolio, S.P. Nolan, Indenyl and allyl Palladate complexes bearing N-heterocyclic Carbene ligands: an easily accessible class of new anticancer drug candidates, Eur. J. Inorg. Chem. 2022 (2022) e202200103, https://doi.org/10.1002/ejic.202200103.
[13] O. Dömötör, F. Binacchi, N. Ribeiro, N. Busto, J. Gonzalez-García, E. Garcia-España, I. Correia, É.A. Enyedy, J. Hamacek, A. Terenzi, N. Basílio, G. Barone, I. Cavaco, T. Biver, How reliable is the evaluation of DNA binding constants? Insights and best practices based on an inter-laboratory fluorescence titration study, Spectrochimica Acta Part A: Molecular and Biomolecular Spectroscopy 327 (2025) 125354, https://doi.org/10.1016/j.saa.2024.125354.
[14] R.D. Wells, J.E. Larson, R.C. Grant, B.E. Shortle, C.R. Cantor, Physicochemical studies on polydeoxyribonucleotides containing defined repeating nucleotide sequences, J. Mol. Biol. 54 (1970) 465–497, https://doi.org/10.1016/0022-2836(70)90121-X.
[15] B. Janik, Physicochemical Characteristics of Oligonucleotides and Polynucleotides, Springer, New York, NY, 1971, pp. 76–95.
[16] W. Mueller, D.M. Crothers, Eur. J. Biochem. 54 (1975) 267, https://doi.org/10.1111/j.1432-1033.1975.tb04137.x.
[17] P. Gans, A. Sabatini, A. Vacca, Investigation of equilibria in solution. Determination of equilibrium constants with the HYPERQUAD suite of programs, Talanta 43 (1996) 1739–1753, https://doi.org/10.1016/0039-9140(96)01958-3.
[18] G. Cohen, H. Eisenberg, Viscosity and sedimentation study of sonicated DNA–proflavine complexes, Biopolymers 8 (1969) 45–55, https://doi.org/10.1002/bip.1969.360080105.
[19] A.D. Becke, Density-functional exchange-energy approximation with correct asymptotic behavior, Phys. Rev. A 38 (1988) 3098–3100, https://doi.org/10.1103/PhysRevA.38.3098.
[20] C. Lee, W. Yang, R.G. Parr, Development of the Colle-Salvetti correlation-energy formula into a functional of the electron density, Phys. Rev. B 37 (1988) 785–789, https://doi.org/10.1103/PhysRevB.37.785.
[21] E. van Lenthe, E.J. Baerends, J.G. Snijders, Relativistic total energy using regular approximations, J. Chem. Phys. 101 (1994) 9783–9792, https://doi.org/10.1063/1.467943.
[22] L. Orian, W.J.V. Zeist, F.M. Bickelhaupt, Linkage isomerism of nitriles in rhodium half-Sandwich Metallacycles, Organometallics 27 (2008) 4028–4030, https://doi.org/10.1021/om8004614.
[23] L. Orian, L.P. Wolters, F.M. Bickelhaupt, In silico Design of Heteroaromatic Half-Sandwich RhI catalysts for acetylene [2+2+2] Cyclotrimerization: evidence of a reverse Indenyl effect, Chem. A Eur. J. 19 (2013) 13337–13347, https://doi.org/10.1002/chem.201301990.
[24] L. Orian, M. Swart, F.M. Bickelhaupt, Indenyl effect due to metal slippage? Computational exploration of rhodium-catalyzed acetylene [2+2+2] Cyclotrimerization, Chem. Phys. Chem. 15 (2014) 219–228, https://doi.org/10.1002/cphc.201300934.
[25] M. Bortoli, F. Zaccaria, M. Dalla Tiezza, M. Bruschi, C. Fonseca Guerra, F. M. Bickelhaupt, L. Orian, Oxidation of organic diselenides and ditellurides by H2O2 for bioinspired catalyst design, Phys. Chem. Chem. Phys. 20 (2018) 20874–20885, https://doi.org/10.1039/C8CP02748J.
[26] M. Dalla Tiezza, F.M. Bickelhaupt, L. Orian, Group 9 Metallacyclopentadienes as key intermediates in [2+2+2] alkyne Cyclotrimerizations. Insight from Activation Strain Analyses, Chem. Phys. Chem. 19 (2018) 1766–1773, https://doi.org/10.1002/cphc.201800178.
[27] M. Dalla Tiezza, F.M. Bickelhaupt, L. Orian, Half-Sandwich metal-catalyzed alkyne [2+2+2] cycloadditions and the slippage span model, ChemistryOpen 8 (2019) 143–154, https://doi.org/10.1002/open.201800191.
[28] A. Madabeni, P.A. Nogara, M. Bortoli, J.B.T. Rocha, L. Orian, Effect of methylmercury binding on the peroxide-reducing potential of cysteine and Selenocysteine, Inorg. Chem. 60 (2021) 4646–4656, https://doi.org/10.1021/acs.inorgchem.0c03619.
[29] E.J. Baerends, D.E. Ellis, P. Ros, Self-consistent molecular Hartree—Fock—slater calculations I. The computational procedure, Chem. Phys. 2 (1973) 41–51, https://doi.org/10.1016/0301-0104(73)80059-X.
[30] G. te Velde, F.M. Bickelhaupt, E.J. Baerends, C. Fonseca Guerra, S.J.A. van Gisbergen, J.G. Snijders, T. Ziegler, Chemistry with ADF, J. Comput. Chem. 22 (2001) 931–967, https://doi.org/10.1002/jcc.1056.
[31] O. Trott, A.J. Olson, AutoDock Vina: improving the speed and accuracy of docking with a new scoring function, efficient optimization, and multithreading, J. Comput. Chem. 31 (2010) 455–461, https://doi.org/10.1002/jcc.21334.
[32] M. Heydari, M.E. Moghadam, A. Tarlani, H. Farhangian, DNA as a target for anticancer Phen-imidazole Pd(II) complexes, Appl. Biochem. Biotechnol. 182 (2017) 110–127, https://doi.org/10.1007/s12010-016-2314-2.
[33] S.K.J. Shaikh, R.R. Kamble, S.M. Somagond, H.C. Devarajegowda, S.R. Dixit, S. D. Joshi, Tetrazolylmethyl quinolines: design, docking studies, synthesis, anticancer and antifungal analyses, Eur. J. Med. Chem. 128 (2017) 258–273, https://doi.org/10.1016/j.ejmech.2017.01.043.
[34] N. Shahabadi, L. Ghaffari, Z. Mardani, F. Shiri, Experimental and molecular docking studies on the interaction of a water-soluble Pd(II) complex containing β-amino alcohol with calf Thymus DNA, Biol. Trace Elem. Res. 200 (2022) 1988–2000, https://doi.org/10.1007/s12011-021-02803-1.
[35] A. Zianna, G. Geromichalos, A.-M. Fiotaki, A.G. Hatzidimitriou, S. Kalogiannis, G. Psomas, Palladium(II) complexes of substituted Salicylaldehydes: synthesis, characterization and investigation of their biological profile, Pharmaceuticals 15 (2022), https://doi.org/10.3390/ph15070886.
[36] E.F. Pettersen, T.D. Goddard, C.C. Huang, G.S. Couch, D.M. Greenblatt, E.C. Meng, T.E. Ferrin, UCSF chimera—a visualization system for exploratory research and analysis, J. Comput. Chem. 25 (2004) 1605–1612, https://doi.org/10.1002/jcc.20084.
[37] J.B. Chaires, A thermodynamic signature for drug–DNA binding mode, Arch. Biochem. Biophys. 453 (2006) 26–31, https://doi.org/10.1016/j.abb.2006.03.027.
[38] T. Hidalgo, D. Fabra, R. Allende, A.I. Matesanz, P. Horcajada, T. Biver, A. G. Quiroga, Two novel Pd thiosemicarbazone complexes as efficient and selective antitumoral drugs, Inorg. Chem. Front. 10 (2023) 1986–1998, https://doi.org/10.1039/D2QI02424A.
[39] A. Madabeni, T. Scattolin, E. Bortolamiol, F. Visentin, L. Orian, Reactivity of palladium(II)-η3-allyl complexes with Chalcogenolates: a density functional study of their antitumor implications, Organometallics 43 (2024) 954–962, https://doi.org/10.1021/acs.organomet.3c00514.